npj | climate and atmospheric science

Article

Published in partnership with CECCR at King Abdulaziz University

https://doi.org/10.1038/s41612-025-01297-1

Predictable atmospheric circulation driver of Eurasian winter temperatures

Nick J. Dunstone[1] ✉, Chaofan Li[2], Doug M. Smith[1], Steven C. Hardiman[1], Leon Hermanson[1], Zu Luo[3], Adam A. Scaife[1,4], Rhidian Thomas[5,6], Lin Wang[2] & Tim Woollings[5]

In contrast to global warming trends, much of Eurasia experienced a winter cooling trend over 1990–2014. Some studies have proposed a causal link between this regional cooling, particularly strong over Siberia, to coincident reductions in Arctic sea-ice extent. However, free-running historical climate models overwhelmingly simulate a forced Eurasian warming signal, leading other studies to suggest that internal variability explains the observed cooling. Here, we use retrospective seasonal climate predictions to highlight a robust dynamical link between Siberian cooling and upstream north-east Atlantic atmospheric circulation changes. Examining the interannual predictability of these circulation patterns, we find spuriously weak but skilful model signals. When these weak dynamical signals are corrected, stronger low-frequency variability in downstream Siberian temperature also emerges, with half of the observed 1990–2014 cooling simulated. Our results suggest that Eurasian decadal climate variability is at least partly driven by a predictable atmospheric circulation response to slowly evolving boundary conditions.

The Earth's global mean near-surface temperature continues to rise, with 2024 being the first year to temporarily exceed 1.5 °C above pre-industrial levels[1]. As expected, however, regional temperatures often show significantly larger variability due to changes in atmospheric circulation patterns, which can either mask or exaggerate underlying anthropogenic warming trends. These can either result from internally generated atmospheric variability and/or external drivers of the climate system. It is essential, therefore, to study and understand the drivers and predictability of recent regional climate variability so that we can make more confident and skilful future regional climate predictions to inform mitigation and adaptation planning.

The observed decadal Eurasian winter cooling that straddled the end of the 20th and the start of the 21st centuries (Fig. 1a) is a key example of regional climate variability opposing the general global warming trend[2], with the Siberian region in particular cooling by −1.1 °C/decade over 1990–2014 (Fig. 1b). This was associated with a strengthening of the Siberian High[3] and an amplification of the East Asian winter monsoon[4]. Over approximately the same period, a strong regional warming occurred in the Arctic and was particularly pronounced over the Barents-Kara Sea region (Fig. 1a) where there was also a strong decrease in autumn-winter sea-ice extent. The coincidence of these events, often referred to as the "warm Arctic-cold Eurasia" (WACE) pattern[5], led to speculation at the time that this behaviour could be an emerging climate change signal[6,7], with amplified Arctic warming driving mid-latitude Eurasian cooling[8]. Many observational and modelling studies have investigated the WACE pattern, but there is little consensus about the cause of the cooling[9–11]. On the one hand, observational studies[12] and some modelling studies undertaking idealised perturbation experiments[13,14] find evidence in support of a causal link with reduced Arctic sea-ice driving a cooling over Eurasia. Other studies, however, find limited evidence[15] or point to different causal relationships whereby low-frequency variability in atmospheric dynamics is driving both Eurasian cooling and amplifying Arctic sea-ice loss[10,16–18]. Furthermore, coordinated multi-model studies on the impact of Arctic sea-ice decline from the Polar Amplification Model Intercomparison Project (PAMIP[19]) have found only weak dynamical responses of the North Atlantic extra-tropical jet and little consistent Eurasian cooling response[20,21]. Indeed, perturbation experiments with large Arctic sea-ice loss can produce a thermodynamic warming signal that overwhelms the associated dynamical cooling signal[22,23].

The most complete simulations of historical climate with realistic external forcings from the sixth Coupled Model Intercomparison Projects (CMIP6[24]), which we revisit below, show negligible evidence for an externally forced cooling signal over central Eurasia[25]. We also now know that the strong Eurasian cooling signal has disappeared (Fig. 1b) over the decade

[1]Met Office Hadley Centre, Exeter, UK. [2]State Key Laboratory of Earth System Numerical Modeling and Application and Center for Monsoon System Research, Institute of Atmospheric Physics, Chinese Academy of Sciences, Beijing, PR China. [3]College of Oceanography & Key Laboratory of Marine Hazards Forecasting, Ministry of Natural Resources, Hohai University, Nanjing, PR China. [4]University of Exeter, Exeter, UK. [5]University of Oxford, Oxford, UK. [6]University of Reading, Reading, UK. ✉e-mail: nick.dunstone@metoffice.gov.uk

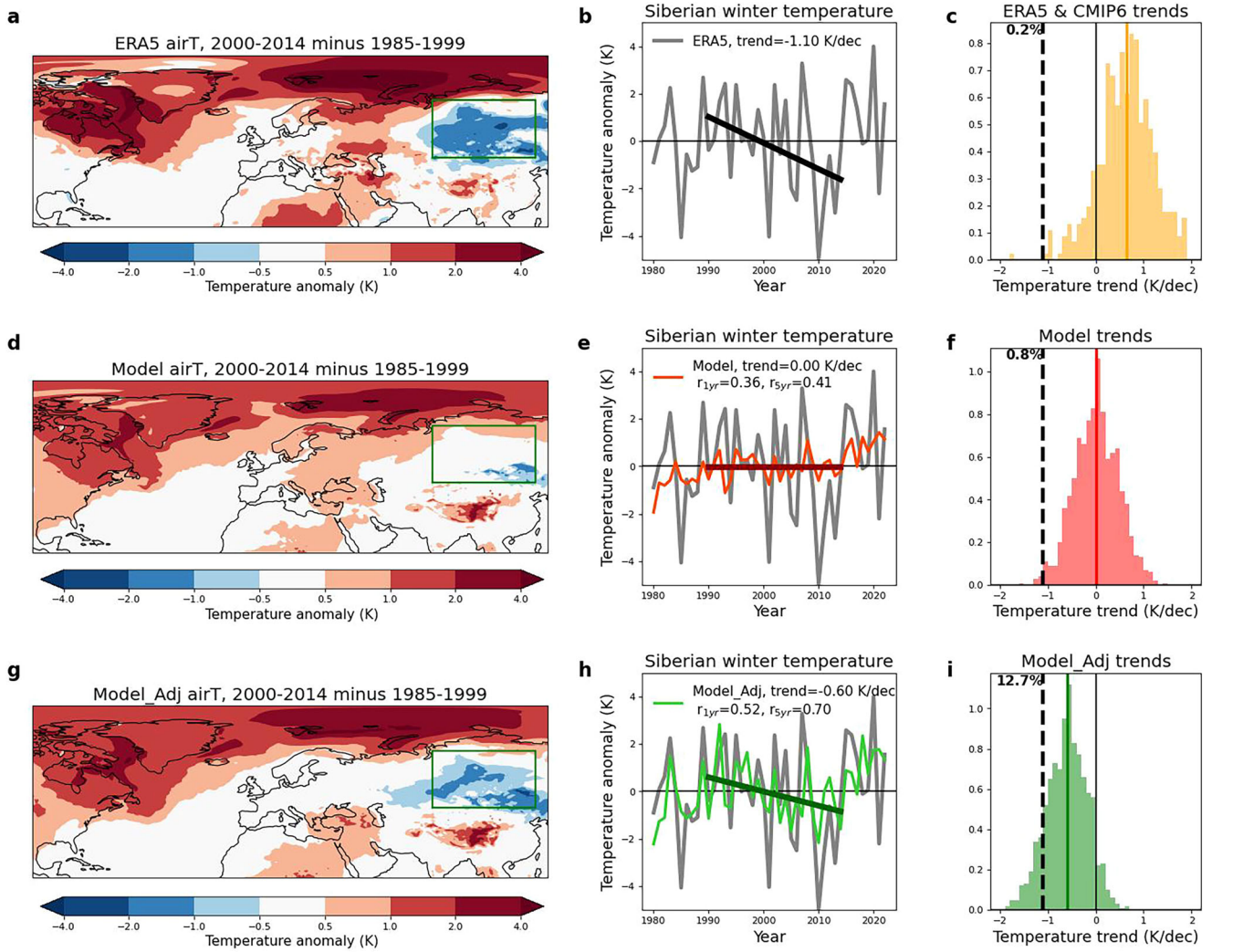

Fig. 1 | Observed and simulated decadal temperature trends over Eurasia. **a** observed ERA5 near-surface air temperature difference and Siberian temperature timeseries (**b**) with the trend plotted calculated over the 25 year period 1990–2014 as used in previous studies (e.g., Wang and Chen[41]). **c** distribution of the 462 CMIP6 historical simulations (see Methods) of Siberian temperature trends with the vertical dashed line showing the ERA5 reanalysis trend. **d** DePreSys3 ('model') ensemble mean initialised on 1st November predicting winter (forecast months 2–4, December–February), near-surface air temperature difference and Siberian temperature timeseries (**e**) with the distribution of 1000 possible permutations (Methods) of model ensemble member Siberia temperature trends (**f**) with the black dashed vertical line showing the observed trend. **g–i** as panels **d**-**f** but now for the 'adjusted' ensemble that accounts for spuriously weak model circulation signals (see "Methods", text and Fig. 3).

since 2015 and central Eurasia has been warming at a rate similar to the Northern Hemisphere average[26], despite continued Arctic warming and sea-ice loss. These findings therefore led to the suggestion that the observed cooling was in fact largely a result of internal variability generating synchronous changes over Eurasia and the Arctic[27–30].

Another possibility, however, is that current climate models may underestimate the strength of forced atmospheric circulation signals over Eurasia and that they might be predictable. Indeed, several studies using retrospective seasonal climate predictions (hereafter hindcasts) have shown evidence for predictable but spuriously weak winter circulation signals in the North Atlantic Oscillation (NAO), upstream of Eurasia[31–34]. Here we use seasonal predictions to explore their simulation of the Eurasian strong cooling period and assess whether atmospheric circulation signals are underestimated.

Results

Observed and modelled trends

We consider winter (December–February) seasonal predictions, from hindcasts starting on 1st November each year from 1981 to 2022 using the Met Office DePreSys3 (hereafter the 'model') near-term prediction system[33] (see "Methods") with 40 ensemble members. As seasonal predictions are initialised from our best estimate of the current conditions in the atmosphere, ocean, and cryosphere, they have knowledge of the current state of the slowly evolving components of the climate system. However, with a lead-time of 1 month the ensemble loses deterministic atmospheric predictability of the synoptic evolution of mid-latitude climate. Seasonal predictions therefore give us the opportunity to study the impact of slowly evolving signals in the climate system on atmospheric variability impacting Eurasia. We first explore whether these hindcasts improve the prediction of Eurasian surface temperature relative to uninitialized CMIP6 historical simulations, which are forced only by changing external forcings alone.

Analysis of 38 free-running CMIP6 historical models (Fig. 1c, see Methods) shows an average warming trend for 1990–2014 over Siberia of +0.64 C/dec (cf -1.1 C/dec observed). Of the 462 individual uninitialised CMIP6 ensemble members, only one member (0.2%) simulates a cooling as strong as that observed. However, it is important to note that because we have pre-selected the strong cooling period in the observations, with no

a-priori information on its location or timing, that we should not treat this as a probability of occurrence[35]. That said, the fact that only 13% of CMIP6 members simulate a Siberian cooling trend at all suggests that any strength of Siberian cooling is not a robust response to external forcings in these coupled ocean-atmosphere climate models.

Examining trends from the model (DePreSys3 near-term prediction system) ensemble, we find on average zero (0.0 C/dec) Siberian warming trend (Fig. 1d and e). Exploring individual model ensemble members to generate a distribution of possible model trends, using resampling of the members (see "Methods"), we find that approximately half (48%) of members exhibit a cooling trend but only 0.8% of model sample trends are as large as the observed trend (Fig. 1f). Hence the initialised model does not simulate an overall warming trend and thus improves upon the uninitialized CMIP6 historical simulations (which we consider no further in this paper), but the ensemble mean does not capture the observed cooling. In summary, our analysis suggests that the observed Siberian cooling could be an example of relatively rare internal variability and/or errors in the model's response to forcing (e.g., either from external forcings and/or from slowly evolving components of the climate system that we initialise in the model hindcasts) over this period. We keep both these possibilities in mind as we now explore the large-scale circulation associated with the Eurasian cooling. Note that we will return later in this paper to discuss the results shown in Fig. 1g–i, once we have explored the dynamical circulation drivers and their model simulation.

Large-scale dynamical circulation changes

Decadal changes in the observed large-scale atmospheric circulation, coincident with the Eurasian cooling, are explored for the upper-troposphere zonal and meridional winds (Fig. 2a and b). In 250 hPa zonal winds, we find a strong dipole over Eurasia, with weakening in the westerly flow over high latitudes and a strengthening over mid-latitudes. Dynamically this corresponds to weakening (reduction in the eastward extent) of the extratropical jet and a northward shift of the sub-tropical jet. The longitudes of the strongest centres of this dipole pattern are located over Europe (Scandinavian and the Mediterranean) and eastern Asia (Siberia and China), with this longitudinal structure implying a strong meridional circulation component. We see this when we examine the 250 hPa meridional wind differences, where we find a striking Rossby wave structure across Eurasia, with alternating centres crossing the North Atlantic to Eurasia. This is similar to the wave-train previously identified[36] and corresponds to positive geopotential height anomalies located over the Ural Mountains during the later period[37]. This expands and amplifies the climatological Siberian High, with more persistent atmospheric blocking, and favours northerly advection of colder Arctic air into Siberia.

To address whether these observed upper-level circulation signals correspond to a commonly occurring pattern of interannual variability we perform a joint (multivariate) Empirical Orthogonal Function (EOF) analysis using the zonal and meridional winds over 1980–2022 and the domain shown in Fig. 2. We find that the second joint-EOF (Fig. 2c and d), explaining 16% of the interannual variance, matches very closely the patterns we have already described (in Fig. 2a and b). We note that the signals over the western North Atlantic, seen in Fig. 2a are removed in this second joint-EOF, as they correspond to meridional shifts in the extratropical jet associated with the higher-frequency interannual behaviour in the North Atlantic Oscillation (NAO) which is represented by the first joint-EOF (not shown). Instead, the second joint-EOF very well picks up the circulation changes across Eurasia which, as we will see, are more closely related to the lower-frequency changes in the strength of the jet[38,39].

To further investigate whether these observed large-scale circulation changes also drive those model ensemble member combinations that have the strongest Siberian cooling trends, we repeat our analysis using the 2% of model members that simulate a strong <−1.0 °C/dec cooling trend (close to the observed −1.1 °C/dec). Interestingly, we find very similar large-scale circulation differences, with changes in both zonal (Fig. 2e) and meridional (Fig. 2f) winds similar to that observed (Fig. 2a and b). As expected, they are somewhat weaker, especially for the meridional winds which also appear to be shifted approximately 10–15 degrees east compared to that observed.

We further investigate the relationship between Eurasian temperature and circulation changes by defining a European zonal jet dipole index (EZJD, green boxes in Fig. 2a, c and e) and relate this to the Siberian temperature trend across all model samples (Fig. 2g). We find a robust relationship ($r = 0.58$, $p < 0.001$) highlighting a strong link between upstream dynamical changes in the east North Atlantic extratropical jet and downstream Eurasian temperatures. We again find that the observations are located right on the edge of the cloud of model points—having both a strong EZJD dynamical signal and Siberian cooling.

Predictable but spuriously weak model dynamics

Earlier we showed that the model ensemble mean simulates zero trend for Siberian temperature over the observed Siberia cooling period. However, the fact that it also does not simulate a significant warming, as the uninitialized CMIP6 models do, suggests that the model may be capturing a *predictable* dynamical signal that is acting to oppose the greenhouse gas induced warming signal. Examining the ensemble mean circulation anomalies, we do indeed find very similar dynamical patterns in upper-troposphere winds (Fig. 3a and b) as that observed (Fig. 2a and b), and also to that found in the strongest members (Fig. 2e and f), with both a weakening of zonal winds over high latitude Eurasia and a wave-like structure in meridional winds. However, we note that this forced signal is much weaker and highlight that the colorbar scale is only a half (±2 m/s cf ±4 m/s) of that shown in Fig. 2, revealing that the forced predictable dynamical signal is very much weaker than that observed.

To better understand the strength and predictability of these key circulation anomalies, we examine the interannual correlation skill over 1981–2022 (Fig. 3c and d). We find significant skill in the model ensemble mean predicting the observed variability (model-obs skill), in the same key locations of the dynamical anomalies we have identified, in both zonal and meridional winds associated with Siberian cooling. For meridional winds, we also find some weaker regions of negative skill, which is a consequence of the earlier identified model wave phase shift relative to that observed. A key question is whether these predicted Eurasian dynamical signals are of the correct amplitude relative to that observed, as there is reason to believe from studies of the winter NAO that extratropical circulation signals may be spuriously weak in current climate models[32–34]. We explore this by calculating the skill of the model in predicting itself, a single withheld ensemble member predicted by the remaining 39 members, a robust estimate of which can be obtained via bootstrap resampling. The resulting model-model skill maps (Fig. 3e and f) are largely devoid of skill over Eurasia, in sharp contrast to model-obs maps (Fig. 3c and d), with almost no locations with correlation coefficient of $r > 0.2$ in either zonal or meridional winds. The ratio of the model-obs to model-model skill gives us the ratio of predictable components[32] (RPC) and is plotted in Fig. 3g and h. Regions where RPC»1 are indicative of underconfidence, whereby the model has higher skill at predicting the observed circulation than its own and hence suggesting that the model may have spuriously weak dynamical signals. We find that the same regions of zonal and meridional winds associated with the Siberian cooling period are highlighted by this analysis with RPC > 1. For comparison, we note that this in contrast to some other low latitude regions, e.g., south-east North America, where the model skilfully predicts both the observed variability and itself (and hence RPC ~ 1).

To explore further we use the previously defined EZJD index upstream of Siberia, with the resulting timeseries plotted in standardised form in Fig. 3i. We find that the model has significant skill ($r = 0.43$, $p = 0.004$) in predicting the interannual EZJD variability. However, we also note that the EZJD exhibits low-frequency decadal variability, including a negative trend

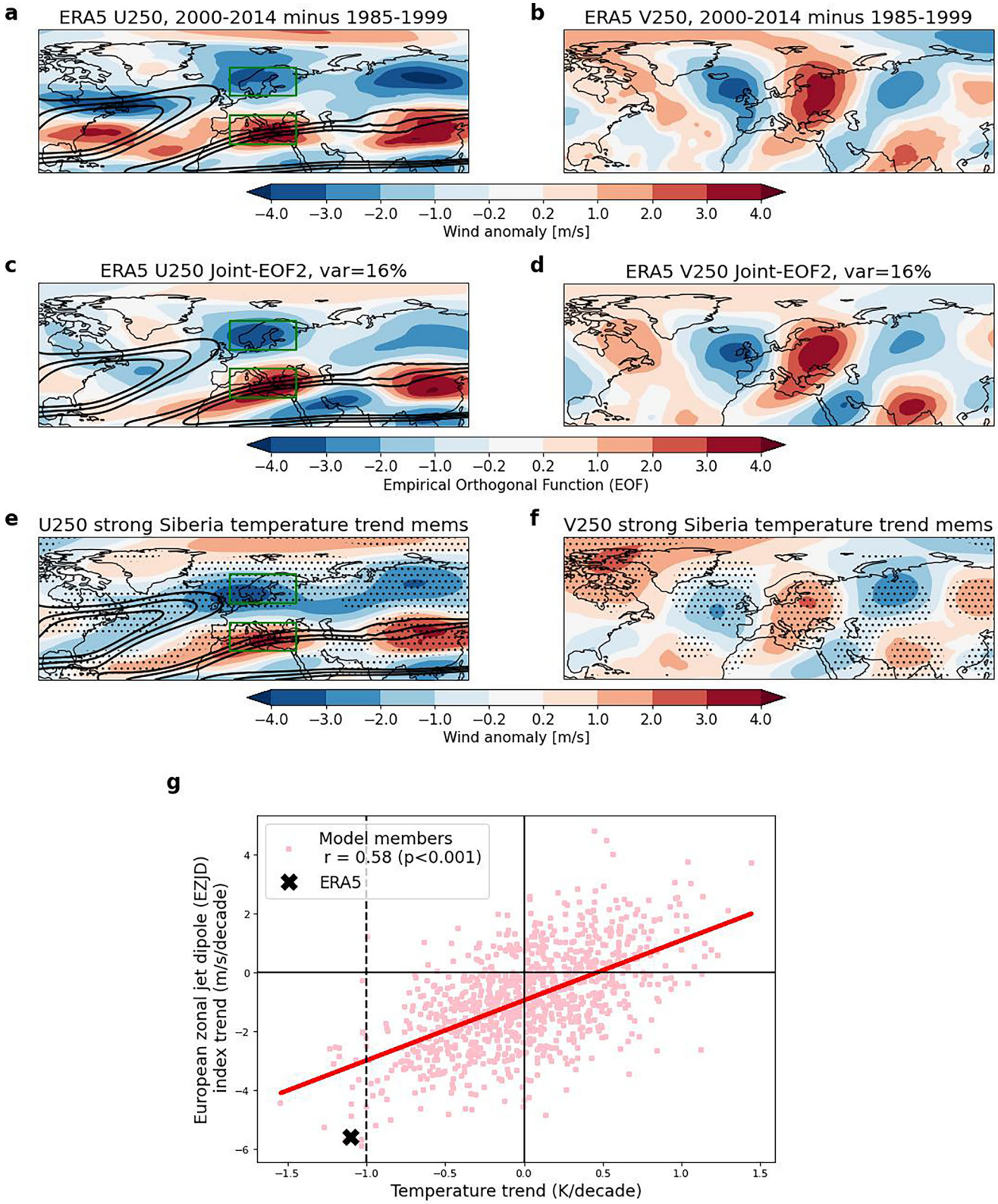

Fig. 2 | Dynamical circulation changes in observations and model members. Observed differences 2000–2014 minus 1985–1999 in observed ERA5 upper troposphere 250 hPa zonal **a** and meridional (**b**) winds. **c**, **d** The second Empirical Orthogonal Function (EOF) from a joint EOF analysis of 250 hPa zonal and meridional winds, calculated over the domain shown and years 1980–2022. **e**, **f** The mean of ensemble member resamples that produce the strongest model Siberian temperature trends (those 19 members from 1000 resamples that have <−1.0 K/dec as shown by dashed vertical line in **g**), with stippling showing locations where this signal is significantly different from the mean of all (unconditioned) ensemble member resamples according to a one-sided Student's *t* test at the 95% confidence level. **g** Siberian temperature trends (1990–2014) are plotted against the EZJD index (highlighted by the green boxes on **a**, **c**, **e**) for each of 1000 model member resamples along with the ERA5 reanalysis value. Contours in **a**, **c**, **e** show the climatological ERA5 250 hPa zonal winds to highlight locations of the mid-latitude jets.

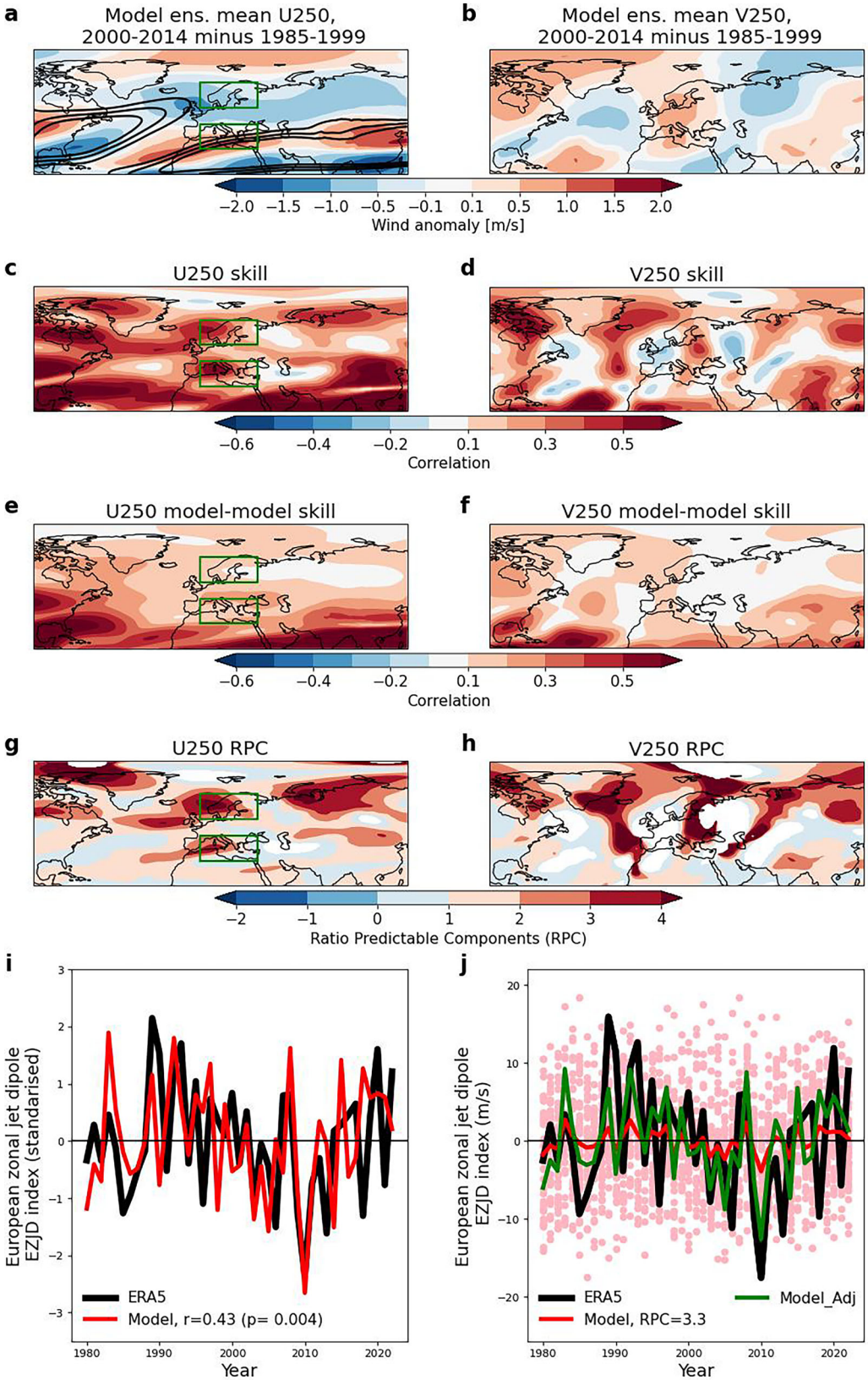

Fig. 3 | A predictable dynamical signal which is spuriously weak. a, **b** zonal and meridional 250 hPa wind differences (as in Fig. 2e and f) but now for the ensemble mean of all model members and plotted with half of the colour bar range, to highlight the similar spatial pattern but weak amplitude of the forced circulation signal. correlation skill at gridpoints of the model ensemble mean predicting the observed ERA5 interannual variability in zonal (**c**) and meridional winds (**d**). **e**, **f** the corresponding skill of the model predicting itself (see Methods). **g**, **h** the ratio of predictable components (RPC, see Methods) where values RPC > 1 suggest the presence of spuriously weak models circulation signals. **i** standardised timeseries of the observed and predicted European zonal jet dipole (EZJD) index. **j** absolute EZJD values (m/s) are plotted for the ensemble mean (red), ERA5 reanalysis (black) along with individual ensemble members (pink circles) and the adjusted ensemble using the matching method (see text and Methods) is shown in green.

over 1990–2014, which is also well simulated by the model ensemble mean, with a 5-year running mean smoothed timeseries (not shown) being even more highly correlated ($r = 0.75$). Despite the significant correlation with the observed EZJD temporal variability, when we plot this in absolute units of m/s (Fig. 3j) we find that the model ensemble mean signal is very weak in amplitude (red line), consistent with the RPC map in Fig. 3g. Put another way, the distribution of individual member EZJD each year (pink circles in Fig. 3j) are very evenly split between positive and negative anomalies and hence the model-model skill of the EZJD is only $r = 0.13$ (cf $r = 0.43$ in model-obs). This results in the EZJD having a RPC = 3.3 (see Methods) which is consistent with, and perhaps stronger than, that found for the NAO in the same model (RPC = 2.3)[33], and again highlights the spuriously weak model dynamical signals.

Adjusting the dynamics and re-examining Eurasian cooling trends

We can adjust the model dynamical signal, by inflating it to account for the spuriously weak dynamical signal and then use a 'member matching' methodology[40] to re-examine the Siberian temperature trends. First, we inflate the model EZJD signal by the ratio of predictable signals (see Methods) resulting in the green line ('Model_Adj', Fig. 3j) with higher amplitude. We can then use the inflated EZJD, along with a bootstrap resampling from the estimated internal variability (see Methods), to pick individual ensemble members (pink circles in Fig. 3j) each year that happen, by chance, to be the closest match. This gives us a distribution of 'adjusted' model members that accounts for the spuriously weak model dynamics, which we can then use to probe the downstream impacts on temperatures over Siberia.

Using our adjusted ensemble, we recalculate the map of Eurasia temperature change (Fig. 1g) to reveal a much stronger cooling difference between the early and late period, especially over Siberia. We also find stronger warming over much of the Arctic, especially the Barents-Kara seas region, in better agreement with that observed. The 1990–2014 Siberian temperature trend (Fig. 1h) now reveals a robust cooling of −0.60 K/dec (cf zero trend originally) which is approximately half the strength of the observed cooling. Furthermore, the distribution of trends in the new adjusted ensemble distribution (Fig. 1i) shows that 90% of samples now produce a cooling trend (cf 48% originally). Importantly, the probability of a cooling trend as strong as that observed has increased by over an order of magnitude in the adjusted model, from 0.8 to 12.7%, making it now a much more plausible sample from internal variability. Additionally, we also find that the interannual Siberian temperature skill increases to $r = 0.52$ (from $r = 0.36$) and the low-frequency 5-year smoothed component of temperature variability is now simulated with a correlation of $r = 0.70$ (from $r = 0.41$). This highlights that when the spuriously weak dynamical variability in the jet dynamics upstream over Europe is accounted for, we can simulate much stronger predictable downstream changes in Siberian surface temperature.

Discussion

We have highlighted a distinct pattern of zonal and meridional atmospheric circulation anomalies associated with Eurasian temperature variability in both observations and in near-term prediction ensemble members with the strongest Siberian cooling trends. Importantly we also find a very similar, but much weaker, predictable signal in the model ensemble mean. Analysis of seasonal predictions reveals significant skill in predicting observed dynamical interannual variations, but that the skill within the model itself (so-called 'perfect predictability') is much lower. This suggests that the model atmosphere is responding too weakly to slowly evolving boundary conditions. Furthermore, it implies that studies examining inter-member spread of large ensembles of historical climate projections[41] likely overestimate the role of internal atmospheric variability.

Some studies[11] present two clearly divergent views regarding the cause of the early 21st century Eurasian cooling, that either internal variability or sea-ice decline are primarily responsible. However, recent studies[18] and reviews[28] have attempted to reconcile these apparently opposing narratives, suggesting that they could co-exist. For example, ref. 28. used the analogy of a roll of a dice to represent internal variability and that slowly varying boundary conditions, such as Arctic sea-ice, had 'loaded' the dice in favour of Eurasian cooling. Our results are in broad agreement with this framework and, extending their analogy, we have demonstrated that the dice in the real-world may well be considerably more 'loaded' than current dynamical climate models simulate, i.e., that the real-atmosphere exhibits a stronger forced dynamical response.

Having identified a forced predictable atmospheric circulation signal, it should in principal be possible to probe which part of the boundary conditions provided to the model has driven this (i.e., the atmosphere, ocean, cryosphere, land surface and external forcings). For example, model perturbation experiments could be undertaken, but these are beyond the scope of the current analysis. Instead, we briefly examine the lagged correlation between the observed principal component timeseries (Fig. 4a), associated with the winter second joint-EOF (Fig. 2a), and fields of meridional 250 hPa winds, sea surface temperature and sea-ice concentration from the preceding October–November. We do this by separately examining the low-frequency (5-year smoothed) and high-frequency (interannual residual) variability (see methods). On the interannual ('high-frequency') timescale (Fig. 4b–d), we find evidence of a Eurasian wave starting in the tropical east Pacific (Fig. 4b) associated with interannual ENSO variability (Fig. 4c) but with no significant connection to Arctic sea-ice anomalies (Fig. 4d). However, on the key low-frequency (5-year mean) timescale, we find that the Eurasian wave is shifted slightly further north and has less obvious connection to the equatorial Pacific (Fig. 4f). Instead, we find relatively strong positive correlations with sea surface temperatures in both the North Atlantic and North Pacific (Fig. 4f), with the typical 'horseshoe pattern' of the positive phase of Atlantic Multidecadal Variability (AMV) and the negative phase of Pacific Decadal Variability (PDV). We also find strong negative correlations with Arctic sea-ice concentrations, particularly over the Barents-Kara Seas region (Fig. 4g). It is not possible to come to any casual conclusions from this analysis of observed behaviour, however these findings are consistent with many previous studies linking low-frequency changes in extratropical SSTs[36,42–44], and/or Arctic sea-ice extent[13,45], with North Atlantic jet behaviour[38], East Atlantic pattern, Eurasian atmospheric circulation[37] and Eurasian surface temperature variability. It remains an open question as to the extent to which Arctic sea-ice variability is a response to atmospheric circulation anomalies, a driver of them, or part of a coupled feedback.

In summary, we have used a large ensemble of near-term predictions to show that Eurasian winter decadal temperature variability is intimately linked with large-scale changes in atmospheric circulation, from the North Atlantic across Eurasia. Our key finding is that the model has skill in predicting this atmospheric circulation, at least on seasonal timescales, but that the predictable dynamical signal in individual model members is spuriously weak and hence results in weak downstream surface Eurasian temperature changes. When we correct for this then we can reproduce stronger Eurasian temperature changes with higher skill. This is promising for the future development of skilful real-time forecasts of Eurasian winter temperatures using improved and/or calibrated climate prediction systems. It also implies that the observed strong Eurasian cooling was not the result of purely unpredictable atmospheric internal variability but was partly a predictable response to slowly evolving boundary conditions. We note that some of these slowly evolving boundary conditions are increasing being linked to changes in external forcings such as emissions of anthropogenic aerosols and greenhouse gases (e.g., in the AMV[46] and PDV[47]). Hence further examination of the forced atmospheric dynamics in large ensembles of uninitialized simulations should be undertaken, where model differences/errors can be exploited to gain further understanding and develop observational constraints[48].

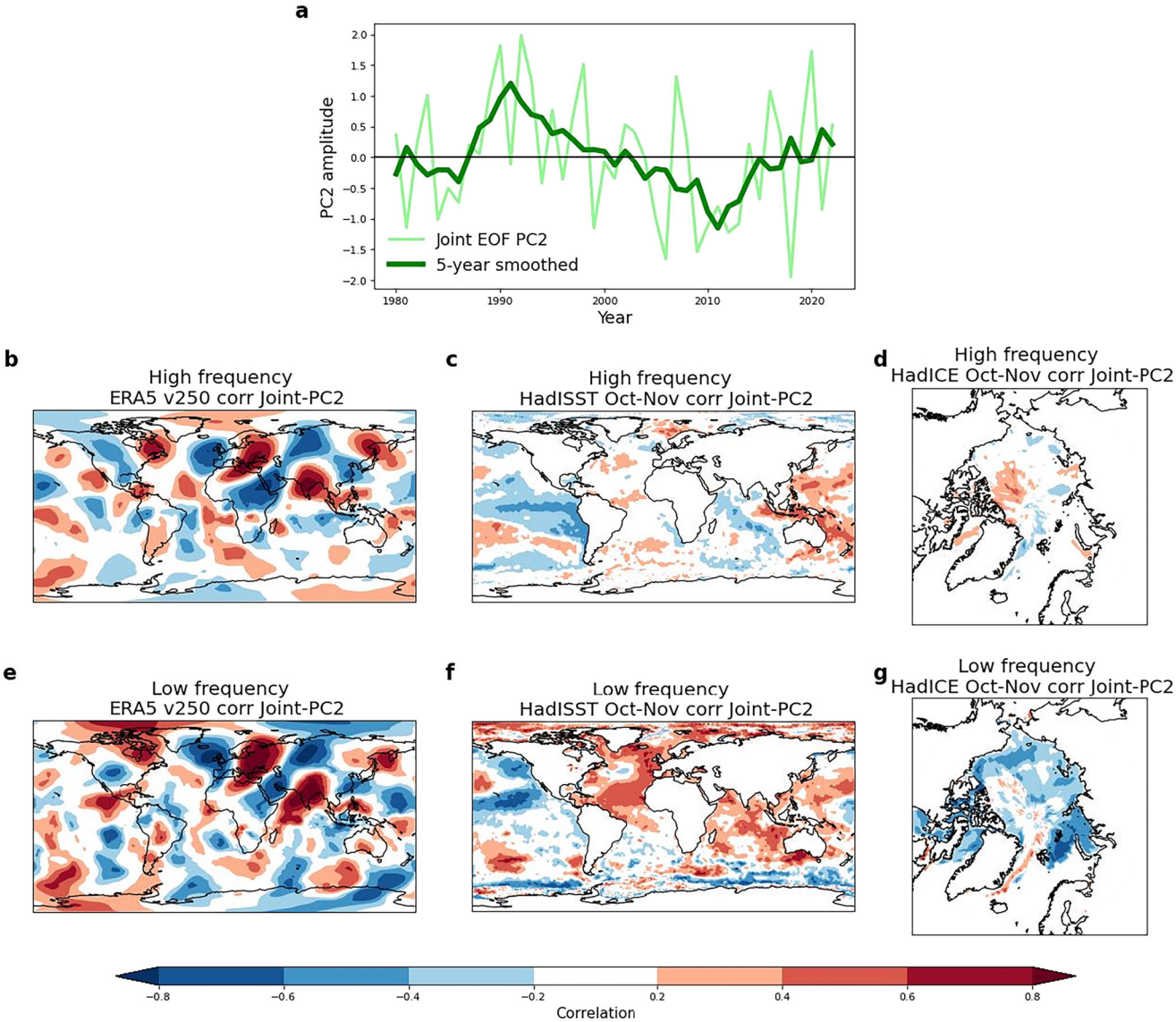

Fig. 4 | Searching for possible drivers of the observed wave. a the timeseries of the joint-EOF PC2 (as shown in Fig. 2a and b) with a 5-year running mean (thick line) used here as the low-frequency timeseries of the Eurasian wave and the residual (not shown) giving the high-frequency timeseries. Maps of the lagged correlation between this high-frequency timeseries of the winter Eurasian wave and the ERA5 fields of meridional 250 hPa winds (**b**) and also the preceding October–November observed HadISST SST (**c**) and sea-ice extent (**d**). **e–g**, as **b–d** but now using the low frequency Eurasian wave timeseries shown in (**a**).

Methods

Initialised prediction system

The near-term climate prediction system used is the Met Office DePreSys3 system[33] referred to here as the 'model'). It is based on the HadGEM3-GC2 coupled climate model[49]. The atmosphere has a horizontal resolution of approximately 60 km (and 85 vertical levels) and an ocean resolution of 0.25° (75 vertical levels). A full-field data assimilating simulation is performed where the climate model is nudged in the ocean, atmosphere and sea-ice components towards observations. In the ocean, temperature and salinity are nudged towards a monthly analysis created using global covariances[50] with a 10 day relaxation timescale. In the atmosphere, temperature and zonal and meridional winds are nudged towards the ERA-Interim[51]/ERA5[52] reanalysis with a six hourly relaxation timescale. Sea ice concentration is nudged towards monthly values from HadISST[53] with a one day relaxation timescale. Hindcasts are started from the 1st November initial conditions of this assimilation simulation and a 40 member ensemble is created using randomly generated seeds to a stochastic physics scheme. The assimilation run, and hindcasts, have full knowledge of external forcing data sets (for example, greenhouse gases, aerosols, ozone, solar and volcanic forcings) as per the CMIP5 protocol[54], and follow the representative concentration pathway (RCP4.5) after 2005.

Uninitialised historical simulations

Uninitialised historical simulations come from the sixth Coupled Model Intercomparison Project (CMIP6[24]). 38 free-running CMIP6 historical models are used with varying ensemble sizes, as recorded in Table 1. In total 462 individual ensemble members are used.

Model member resampling

Individual ensemble members in DePreSys3 are created using random seeds to a stochastic physics scheme and so there is no connection between the same ensemble member number from different start dates (i.e., member #12 in the 1st November 1991 start date ensemble is not linked to member #12 in the 1st November 1992 start date ensemble). We can therefore create a distribution of possible model Siberian temperature trends, whereby for each sample we randomly pick a different ensemble member for each of the DePreSys3 hindcast start dates and concatenate these to make a single timeseries of the same length as the observations. Doing this 1000 times

Table 1 | The names and ensemble size of the individual CMIP6 model uninitialized historical experiments used in this study

Model name	Ensemble size	Model name	Ensemble size
ACCESS-CM2	10	EC-Earth3	33
ACCESS-ESM1-5	40	EC-Earth3-AerChem	2
BCC-CSM2-MR	3	EC-Earth3-CC	10
BCC-ESM1	3	EC-Earth3-Veg-LR	3
CAMS-CSM1-0	1	EC-Earth3-Veg	11
CanESM5	41	FIO-ESM-2-0	3
CanESM5-1	49	GISS-E2-1-G	34
CAS-ESM2-0	4	GISS-E2-1-H	10
CESM2	8	INM-CM4-8	1
CESM2-WACCM	1	INM-CM5-0	10
CMCC-CM2-HR4	1	IPSL-CM6A-LR	32
CMCC-CM2-SR5	11	CM6A-LR-INCA	1
CMCC-ESM2	1	MIROC6	1
FGOALS-f3-L	3	MPI-ESM-1-2-HAM	3
E3SM-1-0	19	MPI-ESM1-2-HR	10
E3SM-1-1	1	MPI-ESM1-2-LR	42
E3SM-1-1-ECA	1	MRI-ESM2-0	1
E3SM-2-0	21	NorCPM1	30
E3SM-2-0-NARRM	5	TaiESM1	2

creates a smooth distribution of possible model Siberian temperature trends (Fig. 1f).

Signal-to-noise calculation

The signal-to-noise paradox is characterised by the ratio of predictable components (RPC) and is calculated as follows[32,34]:

$$RPC = \frac{PC_{obs}}{PC_{mod}} \geq \frac{r_{mo}}{r_{mm}}$$

where the predictable component (PC) of the real world (PC_{obs}) can be conservatively estimated by the correlation between the model ensemble mean and the observations (r_{mo}), and the predictable component of the model can be estimated by the correlation between the model ensemble mean and one of its own members (r_{mm}). A robust estimate of r_{mm} is obtained by bootstrap resampling over 1000 times with each trial picking a single ensemble member for each November start date (we note that in the 40 member DePreSys3 ensemble no properties are transferred across start dates, i.e., ensemble #1 of November 1990 has no relation to ensemble #1 starting in November 1991) and that each member chosen each start date is then excluded from the ensemble mean of that start date which is made with the remaining 39 members.

Adjusted model

We use a 'model matching' methodology, inspired by ref. 40, to correct for the spuriously weak predictable circulation signals (RPC»1) we find in the model (Fig. 3j, red line). We inflate the ensemble mean prediction of the EZJD index by the ratio of predictable signals (RPS). This is essentially the regression between forecast ensemble mean and observed EZJD timeseries, and has a value RPS = 3.8. This results in the inflated ensemble mean signal (green line in Fig. 3j). We then account for the unpredictable internal variability. We estimate this by subtracting the predictable signal, which is diagnosed from the inflated ensemble mean EZJD variance, from the total observed EZJD variance. We create a probability distribution function by taking random samples from a normal distribution with this width, centred on the predictable (inflated) EZJD value each start date (green line in Fig. 3j). We then find the closest original ensemble member (pink circle in Fig. 3j). In this way we construct individual bootstrap trials that are consistent with the predictable (inflated) EZJD signal that corrects for the spuriously weak model dynamical signal, but still samples unpredictable internal variability. We then use this 'adjusted ensemble' to examine the downstream impact on the Siberian temperature trends, producing new distribution of Siberian temperature trends as shown in Fig. 1i.

High and low frequency analysis

We create a 'low frequency' version of the observed principal component timeseries (Fig. 4a), associated with the winter second joint-EOF (Fig. 2a), using a 5-year running mean window, reflecting the start and end of the timeseries. We then subtract this low-frequency version from the original timeseries to obtain a 'high frequency' version. These are then used in the analysis in Fig. 4.

Data availability

ERA5 reanalysis data was downloaded from the European Centre for Medium-Range Weather Forecasts (ECMWF), Copernicus Climate Change Service (C3S) at Climate Data Store (CDS; https://cds.climate.copernicus.eu/). The Coupled Model Intercomparison Project (CMIP6) data is archived and accessible through the Earth System Grid Federation (ESGF). The initialised hindcasts of the Met Office DePreSys3 system are available from the author upon request.

Code availability

Computer code used to produce the figures is available from the corresponding author upon request.

Received: 18 September 2025; Accepted: 7 December 2025;
Published online: 28 January 2026

References

1. Organization (WMO), W. M. State of the Global Climate 2024. https://library.wmo.int/records/item/69455-state-of-the-global-climate-2024.
2. Cohen, J. L., Furtado, J. C., Barlow, M., Alexeev, V. A. & Cherry, J. E. Asymmetric seasonal temperature trends. *Geophys. Res. Lett.* **39**, L04705 (2012).
3. Jeong, J.-H. et al. Recent recovery of the Siberian High intensity. *J. Geophys. Res. Atmos.* **116**, D23102 (2011).
4. Wang, L. & Chen, W. The East Asian winter monsoon: re-amplification in the mid-2000s. *Chin. Sci. Bull.* **59**, 430–436 (2014).
5. Overland, J. E., Wood, K. R. & Wang, M. Warm Arctic - cold continents: climate impacts of the newly open Arctic Sea. *Polar Res.* https://doi.org/10.3402/polar.v30i0.15787 (2011).
6. Cohen, J. et al. Recent Arctic amplification and extreme mid-latitude weather. *Nat. Geosci.* **7**, 627–637 (2014).
7. Francis, J. A., Vavrus, S. J. & Cohen, J. Amplified Arctic warming and mid-latitude weather: new perspectives on emerging connections. *WIREs Clim. Change* **8**, e474 (2017).
8. Outten, S. D. & Esau, I. A link between Arctic sea ice and recent cooling trends over Eurasia. *Clim. Change* **110**, 1069–1075 (2012).
9. Li, C., Stevens, B. & Marotzke, J. Eurasian winter cooling in the warming hiatus of 1998–2012. *Geophys. Res. Lett.* **42**, 8131–8139 (2015).
10. McCusker, K. E., Fyfe, J. C. & Sigmond, M. Twenty-five winters of unexpected Eurasian cooling unlikely due to Arctic sea-ice loss. *Nat. Geosci.* **9**, 838–842 (2016).
11. Cohen, J. et al. Divergent consensuses on Arctic amplification influence on midlatitude severe winter weather. *Nat. Clim. Change* **10**, 20–29 (2020).
12. Yin, M., Yang, X.-Q., Sun, L., Tao, L. & Keenlyside, N. Amplified wintertime Arctic warming causes Eurasian cooling via nonlinear

feedback of suppressed synoptic eddy activities. *Sci. Adv.* **11**, eadr6336 (2025).
13. Honda, M., Inoue, J. & Yamane, S. Influence of low Arctic sea-ice minima on anomalously cold Eurasian winters. *Geophys. Res. Lett.* **36**, L08707 (2009).
14. Mori, M., Watanabe, M., Shiogama, H., Inoue, J. & Kimoto, M. Robust Arctic sea-ice influence on the frequent Eurasian cold winters in past decades. *Nat. Geosci.* **7**, 869–873 (2014).
15. Woollings, T., Harvey, B. & Masato, G. Arctic warming, atmospheric blocking and cold European winters in CMIP5 models. *Environ. Res. Lett.* **9**, 014002 (2014).
16. Blackport, R., Screen, J. A., van der Wiel, K. & Bintanja, R. Minimal influence of reduced Arctic sea ice on coincident cold winters in mid-latitudes. *Nat. Clim. Change* **9**, 697–704 (2019).
17. Warner, J. L., Screen, J. A. & Scaife, A. A. Links between Barents-Kara Sea Ice and the extratropical atmospheric circulation explained by internal variability and tropical forcing. *Geophys. Res. Lett.* **47**, e2019GL085679 (2020).
18. Gong, H. et al. Teleconnection from Arctic warming suppresses long-term warming in central Eurasia. *Sci. Adv.* **11**, eadq9461 (2025).
19. Smith, D. M. et al. The Polar Amplification Model Intercomparison Project (PAMIP) contribution to CMIP6: investigating the causes and consequences of polar amplification. *Geosci. Model Dev.* **12**, 1139–1164 (2019).
20. Smith, D. M. et al. Robust but weak winter atmospheric circulation response to future Arctic sea ice loss. *Nat. Commun.* **13**, 727 (2022).
21. Zheng, C., Wu, Y., Ting, M., Screen, J. A. & Zhang, P. Diverse Eurasian temperature responses to Arctic Sea Ice Loss in models due to varying balance between dynamic cooling and thermodynamic warming. https://doi.org/10.1175/JCLI-D-22-0937.1 (2023).
22. Smith, D. M. et al. Atmospheric Response to Arctic and Antarctic Sea Ice: the Importance of Ocean–Atmosphere Coupling and the Background State. https://doi.org/10.1175/JCLI-D-16-0564.1 (2017).
23. Screen, J. A. The missing Northern European winter cooling response to Arctic sea ice loss. *Nat. Commun.* **8**, 14603 (2017).
24. Eyring, V. et al. Overview of the Coupled Model Intercomparison Project Phase 6 (CMIP6) experimental design and organization. *Geosci. Model Dev.* **9**, 1937–1958 (2016).
25. Sun, C., Zhu, L., Liu, Y., Wei, T. & Guo, Z. CMIP6 model simulation of concurrent continental warming holes in Eurasia and North America since 1990 and their relation to the Indo-Pacific SST warming. *Glob. Planet. Change* **213**, 103824 (2022).
26. Blackport, R. & Screen, J. A. Observed Statistical Connections Overestimate the Causal Effects of Arctic Sea Ice Changes on Midlatitude Winter Climate. https://doi.org/10.1175/JCLI-D-20-0293.1 (2021).
27. Peings, Y. Ural blocking as a driver of early-winter stratospheric warmings. *Geophys. Res. Lett.* **46**, 5460–5468 (2019).
28. Outten, S. et al. Reconciling conflicting evidence for the cause of the observed early 21st century Eurasian cooling. *Weather Clim. Dyn.* **4**, 95–114 (2023).
29. Gong, H., Wang, L., Chen, W. & Wu, R. Time-varying contribution of internal dynamics to wintertime land temperature trends over the Northern Hemisphere. *Geophys. Res. Lett.* **46**, 14674–14682 (2019).
30. Gong, H., Wang, L., Chen, W. & Wu, R. Attribution of the East Asian Winter Temperature Trends During 1979–2018: role of external forcing and internal variability. *Geophys. Res. Lett.* **46**, 10874–10881 (2019).
31. Scaife, A. A. et al. Skillful long-range prediction of European and North American winters. *Geophys. Res. Lett.* **41**, 2514–2519 (2014).
32. Eade, R. et al. Do seasonal-to-decadal climate predictions underestimate the predictability of the real world?. *Geophys. Res. Lett.* **41**, 5620–5628 (2014).
33. Dunstone, N. et al. Skilful predictions of the winter North Atlantic Oscillation one year ahead. *Nat. Geosci.* **9**, 809–814 (2016).
34. Scaife, A. A. & Smith, D. A signal-to-noise paradox in climate science. *Npj Clim. Atmos. Sci.* **1**, 28 (2018).
35. Eade, R., Stephenson, D. B., Scaife, A. A. & Smith, D. M. Quantifying the rarity of extreme multi-decadal trends: how unusual was the late twentieth century trend in the North Atlantic Oscillation? *Clim. Dyn.* **58**, 1555–1568 (2022).
36. Wang, L., Liu, Y., Zhang, Y., Chen, W. & Chen, S. Time-varying structure of the wintertime Eurasian pattern: role of the North Atlantic sea surface temperature and atmospheric mean flow. *Clim. Dyn.* **52**, 2467–2479 (2019).
37. Luo, D. et al. Impact of Ural Blocking on Winter Warm Arctic–Cold Eurasian Anomalies. Part I: Blocking-Induced Amplification. https://doi.org/10.1175/JCLI-D-15-0611.1 (2016).
38. Woollings, T. et al. Contrasting interannual and multidecadal NAO variability. *Clim. Dyn.* **45**, 539–556 (2015).
39. Simpson, I. R., Deser, C., McKinnon, K. A. & Barnes, E. A. Modeled and observed multidecadal variability in the North Atlantic Jet Stream and Its connection to sea surface temperatures. https://doi.org/10.1175/JCLI-D-18-0168.1 (2018).
40. Smith, D. M. et al. North Atlantic climate far more predictable than models imply. *Nature* **583**, 796–800 (2020).
41. Wang, S. & Chen, W. Impact of internal variability on recent opposite trends in wintertime temperature over the Barents–Kara Seas and central Eurasia. *Clim. Dyn.* **58**, 2941–2956 (2022).
42. Liu, Y., Wang, L., Zhou, W. & Chen, W. Three Eurasian teleconnection patterns: spatial structures, temporal variability, and associated winter climate anomalies. *Clim. Dyn.* **42**, 2817–2839 (2014).
43. Luo, D. et al. Winter Eurasian cooling linked with the Atlantic Multidecadal Oscillation. *Environ. Res. Lett.* **12**, 125002 (2017).
44. Patrizio, C. R., Athanasiadis, P. J., Smith, D. M. & Nicolì, D. Ocean-atmosphere feedbacks key to NAO decadal predictability. *Npj Clim. Atmos. Sci.* **8**, 146 (2025).
45. Kug, J.-S. et al. Two distinct influences of Arctic warming on cold winters over North America and East Asia. *Nat. Geosci.* **8**, 759–762 (2015).
46. Booth, B. B. B., Dunstone, N. J., Halloran, P. R., Andrews, T. & Bellouin, N. Aerosols implicated as a prime driver of twentieth-century North Atlantic climate variability. *Nature* **484**, 228–232 (2012).
47. Klavans, J. M. et al. Human emissions drive recent trends in North Pacific climate variations. *Nature* **644**, 684–692 (2025).
48. Smith, D. M. et al. Mitigation needed to avoid unprecedented multi-decadal North Atlantic Oscillation magnitude. *Nat. Clim. Change* **15**, 403–410 (2025).
49. Williams, K. D. et al. The Met Office Global Coupled model 2.0 (GC2) configuration. *Geosci. Model Dev.* **8**, 1509–1524 (2015).
50. Smith, D. M. & Murphy, J. M. An objective ocean temperature and salinity analysis using covariances from a global climate model. *J. Geophys. Res. Oceans.* **112**, C02022 (2007).
51. Dee, D. P. et al. The ERA-Interim reanalysis: configuration and performance of the data assimilation system. *Q. J. R. Meteorol. Soc.* **137**, 553–597 (2011).
52. Hersbach, H. et al. The ERA5 global reanalysis. *Q. J. R. Meteorol. Soc.* **146**, 1999–2049 (2020).
53. Rayner, N. A. et al. Global analyses of sea surface temperature, sea ice, and night marine air temperature since the late nineteenth century. *J. Geophys. Res. Atmos.* **108**, 4407 (2003).
54. Taylor, K. E., Stouffer, R. J. & Meehl, G. A. An Overview of CMIP5 and the Experiment Design. https://doi.org/10.1175/BAMS-D-11-00094.1 (2012).

Acknowledgements

This work was supported by the Met Office Hadley Centre Climate Programme funded by BEIS and Defra. It was also funded by the Met Office Climate Science for Service Partnership (CSSP) China project under the International Science Partnerships Fund (ISPF). LW acknowledges the support of the National Science Foundation of China (42261144687).

Author contributions

N.J.D. led the analysis. N.J.D., C.L., and D.M.S. wrote the first draft of the manuscript. C.L. and Z.L. obtained and analysed the CMIP6 model data. C.L., S.C.H., L.H., Z.L., A.A.S., R.T., L.W., and T.W. contributed to the editing and writing of the manuscript.

Competing interests

The authors declare no competing interests.

Additional information

Correspondence and requests for materials should be addressed to Nick J. Dunstone.

Reprints and permissions information is available at http://www.nature.com/reprints

Publisher's note Springer Nature remains neutral with regard to jurisdictional claims in published maps and institutional affiliations.